National Transportation Safety Board
Office of Research and Engineering
Washington, DC 20594

ERA22FA279

MATERIALS LABORATORY

Factual Report 23-005

June 21, 2023

(This page intentionally left blank)

A. ACCIDENT INFORMATION

Location: Amherstdale, West Virginia
Date: June 22, 2022
Vehicle: Bell UH-1B, N98F
Investigator: Pierre Scarfo, AS-40

B. COMPONENTS EXAMINED

Air diffuser housing, number 2 bearing, housing, oil impellers, retaining plate, rear liner, and aft seal housing assembly, Rear (number 3 and 4) bearing cover, and exhaust diffuser.

C. EXAMINATION PARTICIPANTS

Specialist — Matthew R. Fox, Ph.D.
NTSB
Washington, DC

D. DETAILS OF THE EXAMINATION

Overall views of the submitted components as received are shown in figures 1 through 5. The components included the number 2 bearing and various rotating and non-rotating parts associated with the number 2 bearing and rear compressor shaft assembly shown in figures 1 and 2. Non-rotating components from the aft end of the engine consisted of the number 3 and 4 bearing retaining cover and the exhaust diffuser shown in figures 3 and 4. The remaining submitted components were two power turbine (PT) blade root fragments shown in figure 5.

The components were from an Ozark Aeroworks (formerly Honeywell, Allied Signal, and Textron Lycoming) model T-53-L-11D turboshaft engine. (The civil variant of the engine is the model T53L11A.) A diagram of the engine cross-section is shown in figure 6, where the air flow and bearing locations are indicated. Exploded parts diagrams of the number 2 bearing and associated components are shown in figure 7.

1.0 Number 2 Bearing and Associated Components

The number 2 bearing was received with the outer race and one of the rolling elements separated from the rest of the bearing as shown in figure 2. A closer view of the rolling elements is shown in figure 8. The bearing cage and inner race were intact, and the inner race was darkened with heat tinting. The rolling elements were also heat damaged and flattened on one side consistent with skidding. The outer race, shown in figure 9, was also intact. The raceway had metal deposits on the surface that protruded from the original surface consistent with metal transfer from

the rolling elements. The outer race was slightly heat tinted, but no evidence of pits or spalling damage was observed.

As described in the engine teardown notes, no obstructions were detected in the number 2 bearing oil pressure (supply) tube in the air diffuser housing (see figure 1). However, an obstruction was detected in the oil scavenge tube. Starting at the inlet for the oil scavenge tube, a cannula cleaning brush was inserted approximately 3.1 inches until it met resistance. This location corresponded to a change in tube diameter on the forward side of the air diffuser housing cavity. An abrasive cutting tool was used to cut the tube on inlet side of the diameter change, and the cannula cleaner was inserted at the cut location with no resistance felt for approximately 3.75 inches, a location corresponding to another change in tube diameter. An abrasive cutting tool was used to cut out a section of the scavenge tube on the aft side of the diffuser shown in figure 1, and the tube appeared to be partially obstructed. The cannula cleaning brush was used to push out material in the tube into a sample dish, and the resulting deposit is shown in figure 10. On the outer diameter of the air diffuser housing, an abrasive cutting tool was used to cut an opening near the oil scavenge outlet fitting, and no additional obstructions were observed.

Several of the larger pieces of debris collected from the oil scavenge tube shown in figure 10 were mounted on a stub for analysis using energy dispersive x-ray spectroscopy (EDS). A typical EDS spectrum for the debris is shown in figure 11, where peaks consistent with a low alloy steel were observed. The separated rolling element from the number 2 bearing was also analyzed using EDS, and the resulting spectrum is also shown in figure 11. Both spectra had similar detected elements and relative peak heights.

The forward oil impeller is shown in figure 12. The oil impeller showed heat damage that radiated from the inside diameter with more intense discoloration near the inside diameter and less at the outside diameter. The aft oil impeller showed less heat tinting. Rub damage was observed at the inside diameter of the retaining plate as indicated in the upper image in figure 13, and static contact marks corresponding to contact with the retaining plate were observed on the aft oil impeller also shown in figure 13. According to notes from the engine teardown, the oil holes near the rub damage on the retaining plate were found to be unobstructed.

Close views of the rear liner and the aft seal housing are shown in figures 14 and 15. Circumferential rubbing and heat tinting was observed on the rear liner. The aft seal also showed heat tinting, rubbing, and degradation of the seals.

2.0 Number 3 and 4 Bearing Retaining Cover

The number 3 and 4 bearing retaining cover was recovered in two pieces as shown in figure 3. During the engine teardown, the forward side of the retaining

cover was found secured to the aft end of the exhaust diffuser, and the aft flange piece of the retaining cover was found loose. When compared to an exemplar bearing retaining cover, approximately ½ inch of the outer diameter flange material was missing between the recovered pieces shown in figure 3.

A close view of the flange separation surface at the outside diameter of the forward piece of the number 3 and 4 bearing retaining cover is shown in figure 16. The flange wall thickness was thinned at the separation location, and the thinned edges were rolled inward. The exterior surfaces of the rolled material appeared battered consistent with repeated contact with the separated aft flange piece. The forward end of the aft flange piece also showed thinned material that was rolled inward as shown in figure 17.

On the forward piece of the number 3 and 4 bearing support cover, a piece of rolled flange material at the outside diameter was cut from the remainder of the piece to view the interior surface adjacent to the separation surface, and a view of the surface is shown in figure 18. The interior surface was rough and oxidized consistent with heavy corrosion.

3.0 Exhaust Diffuser

Views of the forward side of the exhaust diffuser are shown in figures 4 and 19, and a cutaway diagram labeling components of the diffuser is shown in figure 20. As shown in the diagram, the exhaust diffuser consisted of an outer cone and a mid cone that were attached at the forward outer flange and an inner cone that was attached to the forward end of the bearing housing support. The outer cone was connected to the bearing housing by four inner struts, and the inner struts were surrounded by an outer strut that was attached to the mid cone and could slide radially within the outer strut fairing on the inner cone.

Clock positions as viewed looking forward were marked on the exhaust diffuser as received, and struts were located at the 3, 6, 9, and 12 o'clock positions as indicated in figure 19. Cracks were observed in multiple locations including the outer struts, inner strut support (outer) flanges (outer cone attachments), inner strut inner flanges (bearing housing support attachments), and the forward end of the inner cone as detailed below.

Each of the outer struts were cracked at the leading edge in the radius between the strut and the flange attaching the strut to the mid cone. Views of cracks in two of these struts are shown in figure 21. Outer struts at the 3 o'clock and 9 o'clock positions also showed impact damage on the counter-clockwise side of the strut near the leading edge. Cracks in struts at the 6, 9, and 12 o'clock positions had a relatively smooth curving path such as the crack shown at the left in figure 21, but the crack at the 3 o'clock position had a discontinuity in the crack path on the side with the impact damage as shown at the right in figure 21. The impact damage at the

6 o'clock position was at the edge of the flange attaching the strut to the mid cone and did not appear to affect the crack path.

Additional cracks were observed in other areas of the outer struts and outer strut fairings. The outer struts at the 3, 9, and 12 o'clock positions were also cracked at the aft radius where the strut transitioned to the flange attached to the mid cone. Outer struts at the 9 o'clock and 12 o'clock positions had spanwise cracks along the forward and aft edges, respectively, near the inner cone. Outer strut fairings at the 3 o'clock and 6 o'clock positions had radial cracks at the aft and forward edges of the fairing, respectively.

Multiple cracks were observed in each of the inner strut support flanges attached to the outer cone. The support flange at the 3 o'clock position shown in figure 22 shows typical crack locations observed on the support flanges. Each of the flanges was cracked at the aft side of the support flange where it was attached to the outer cone, and cracks turned toward the forward direction near the clockwise and counterclockwise edges of the plate. The cracks at the edges of the plate extended further forward at the 3 o'clock and 9 o'clock positions than at the other two positions.

Cracks in the support flanges were also observed near the middle of the flanges around the inner strut attachment weld (see figure 22). At the 3, 6, and 9 o'clock positions, cracks were generally located at the transition radius between the flange and the strut around the forward side of the strut and transitioned radially outward to the toe of the strut attachment weld at the aft side of the strut. Around the inner strut at the 12 o'clock position, the support flange was only cracked through the weld in the aft clockwise quadrant of the strut attachment. The support flange was cracked around the entire perimeter of the inner strut at the 6 o'clock position. At the 3 o'clock position, the support flange was cracked around ¾ of inner strut perimeter. At the 9 o'clock position, the support flange was cracked around the forward and clockwise sides of the inner strut.

To facilitate further examination of the cracked support flanges, the exhaust diffuser housing was cut using a table bandsaw. A radial cut through the outer and mid cones was followed by circumferential cuts through each of the support struts, separating the outer and mid cones from the inner cone and bearing housing support. The inner strut support flanges were then cut using an abrasive cutting tool with cuts intersecting crack tips to facilitate separation of mating fracture surfaces for examination.

The cracks at the aft edges of the support flanges had relatively smooth features across most of the fractures with multiple ratchet marks radiating from the inner surface of the support flange, features consistent with fatigue cracking from

multiple origins at the inner surface.[1] Typical fracture features at the aft edge of the support flange at the 12 o'clock position are shown in figure 23. The fracture surfaces generally had a relatively uniform straw-colored oxide tint under rubbed black deposits from the origin areas to the forward ends of the cracks at the clockwise and counterclockwise sides of the support flange.

Cracks at the middle of the support flange around the inner support attachment generally had a rougher appearance consistent with higher cyclic stresses and showed more rubbing damage from post-fracture recontact. Fracture surfaces generally had irregular multi-colored tint patterns with orange, red, blue, and purple oxide hues such as the fracture surface at the 9 o'clock inner strut position shown in figure 24.

The inner cone had multiple fractures at the forward end of the cone. Radial cracks and fractures in the curved portion between the bearing housing support and the flat front face were located at the 1:00, 4:00, 4:30, 5:00, 7:00, 8:30, 9:00, and 11:30 clock positions with pieces missing at the 12 and 9 o'clock positions. The front face of the inner cone was also fractured radially at the 4 o'clock position. At the corner between the front face and the outside diameter, the cone was fractured circumferentially between 2:00 and 4:30 clock positions. At the inside diameter of the front face, the cone was fractured circumferentially from the 11:30 clock position clockwise to the 5 o'clock position and at the 9 o'clock position. At the inside diameter where the inner cone attached to the bearing housing support, the inner cone was fractured circumferentially from the 5 o'clock position clockwise to the 1 o'clock position.

To facilitate further examination of the inner cone and inner strut inner flange fracture surfaces, the inner cone was sectioned longitudinally at the 3 o'clock and 9 o'clock positions using both a handheld bandsaw and an abrasive cutter, and a view of the inner cone and bearing housing support after sectioning is shown in figure 25. The inner strut inner flange at the 12 o'clock position was fractured around the perimeter of the strut, so it is shown separated from the bearing housing support in figure 25.

Each inner strut was fractured or cracked in the radius where the inner flange transitioned to the inner strut such as the crack indicated at the 6 o'clock position in the right image in figure 25. At the 12 o'clock position, the inner flange was fractured through the transition radius around the forward half of the strut. The fracture transitioned outward to the welded edge of the flange at the aft side of the strut, where the weld was fractured in a shear plane nearly parallel to the flange surface. Views of the separated strut at the 12 o'clock position and the weld fracture at the aft side of the strut flange are shown in figure 26. The fracture features at the forward

[1] A ratchet mark is a small step in the fracture surface formed when two adjacent fatigue cracks originate on slightly offset planes.

end of the fracture had relatively rough features with rubbing damage. Oxides on the surfaces had straw-colored, orange, and red tints. Fracture features at the aft end of the strut at the 12 o'clock position appeared substantially rubbed.

The inner strut inner flanges for the 3, 6, and 9 o'clock positions were each cracked around approximately ¾ of the inner strut perimeter. The inner flange remained intact at the aft end of the inner strut at the 3 o'clock position, and the aft counterclockwise quadrant of the inner flanges remained intact at the 6 o'clock and 9 o'clock positions. Additionally at the 3 o'clock and 6 o'clock positions, welds attaching the inner strut inner flanges to the bearing housing support were cracked at the forward ends of the flanges.

To facilitate further examination of the cracks in the inner strut inner flange radii at the 3, 6, and 9 o'clock positions, an abrasive cutting tool was used to connect the crack tips in the inner flange to separate the crack faces. A view of the outer side of the fracture surfaces after separation are shown in figure 26. The fracture features at each location appeared similar, and representative images of the fracture surfaces at the 6 o'clock position are shown in figure 26. The fracture features had relatively rough features with rubbing damage, and fracture-surface oxides had straw-colored, orange, and red tints.

A view of the bearing housing support with attached piece of the inner cone after sectioning is shown in figure 27. The inner diameter of the inner cone was spot welded to the outer diameter of the bearing housing support near the forward end of the support. Unlabeled arrows in figure 27 point to spot welds in the close-up views of the fracture around the perimeter. The circumferential fracture of the inner cone from the 5 o'clock position clockwise to the 1 o'clock position intersected the forward edges of the spot welds. Additionally, a separate circumferential crack intersecting the forward edges of 5 spot welds was observed at the 3 o'clock position.

A view of fracture features on the inner cone fracture surface at the forward edge of the spot welds are shown in figure 28. The fracture surface had multiple often-intersecting areas with relatively smooth features with curving boundaries, features consistent with fatigue. The fatigue features emanated from the forward edges of individual spot welds consistent with multiple-site fatigue cracks initiating at the spot welds. The fatigue regions had dark gray to black oxides that extended completely or nearly through the inner cone wall thickness in multiple areas. Ratchet marks were observed at each of the origin areas associated with the spot welds such as the two shown in figure 28. An area where the fatigue region extended completely through the inner cone wall is also indicated in figure 28.

4.0 PT Blades

As shown in figure 5, the PT blades were received covered with black sooty deposits. For purposes of this report, the blade fragments were arbitrarily labeled A

and B for reference as shown in figure 5. Blades A and B were fractured approximately 0.24 inch and 0.19 inch from the root platform, respectively, and both blades had a similar groove in the leading edge between the platform and the fracture surface consistent with post-fracture circumferential rub damage.

To facilitate further examination, the blade pieces were submerged in a solution of Alconox detergent and warm water and cleaned using an ultrasonic cleaner. After a preliminary examination, additional deposits on the trailing edge of blade B were removed using a soft-bristle brush dipped in the Alconox solution followed by additional cleaning with the ultrasonic cleaner.

Overall views of the cleaned PT blades are shown in figure 29, and closer views of the fracture surfaces are shown in figure 30. The fracture surface of blade A had relatively rough fracture features consistent with overstress fracture with influence from the cast microstructure. Heat tinting was observed at the leading edge consistent with post-fracture local heating from rubbing contact at the leading edge.

The fracture surface for blade B also had rough fracture features across most of the fracture surface with heat tinting at the leading edge associated with heating from post-fracture rubbing contact. However, an area near the trailing edge had a relatively smoother appearance and had a different tint to the surface oxides. Blade B was further examined using a scanning electron microscope (SEM), and a stitched montage of SEM images of the fracture surface at the trailing edge is shown in the lower image in figure 30. Fatigue striations were observed emanating from a primary origin area located on the convex side of the blade near the trailing edge and from two secondary origin areas on the convex side as shown in the lower image in figure 30. The fatigue region extended to the dashed line boundary shown in figure 30, located approximately 0.243 inch from the blade's trailing edge.

A closer view of the primary origin area is shown in figure 31. Unlabeled arrows indicate local fatigue crack propagation directions emanating from the primary origin that was comprised of a featureless facet at the blade convex surface. No evidence of any anomalies or preexisting damage was observed at the origin area.

Representative fracture features in the fatigue region at increasing distances from the primary origin area are shown in figures 32 to39. Finely-spaced striations on faceted planes were observed in many areas, sometimes separated by more distinct arrest marks such as those shown in figure 38. Forward of the fatigue boundary, fracture features consisted of dimpled features and tear ridges roughly following boundaries in the cast microstructure, such as the area shown in figure 40.

Submitted by:

Matthew R. Fox, Ph.D.
Chief Technical Advisor - Materials

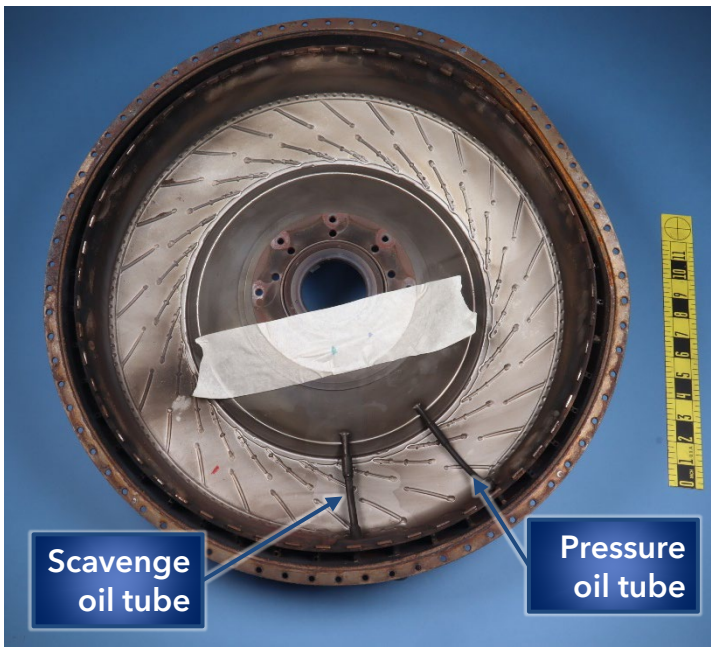

Figure 1. Air diffuser housing as received.

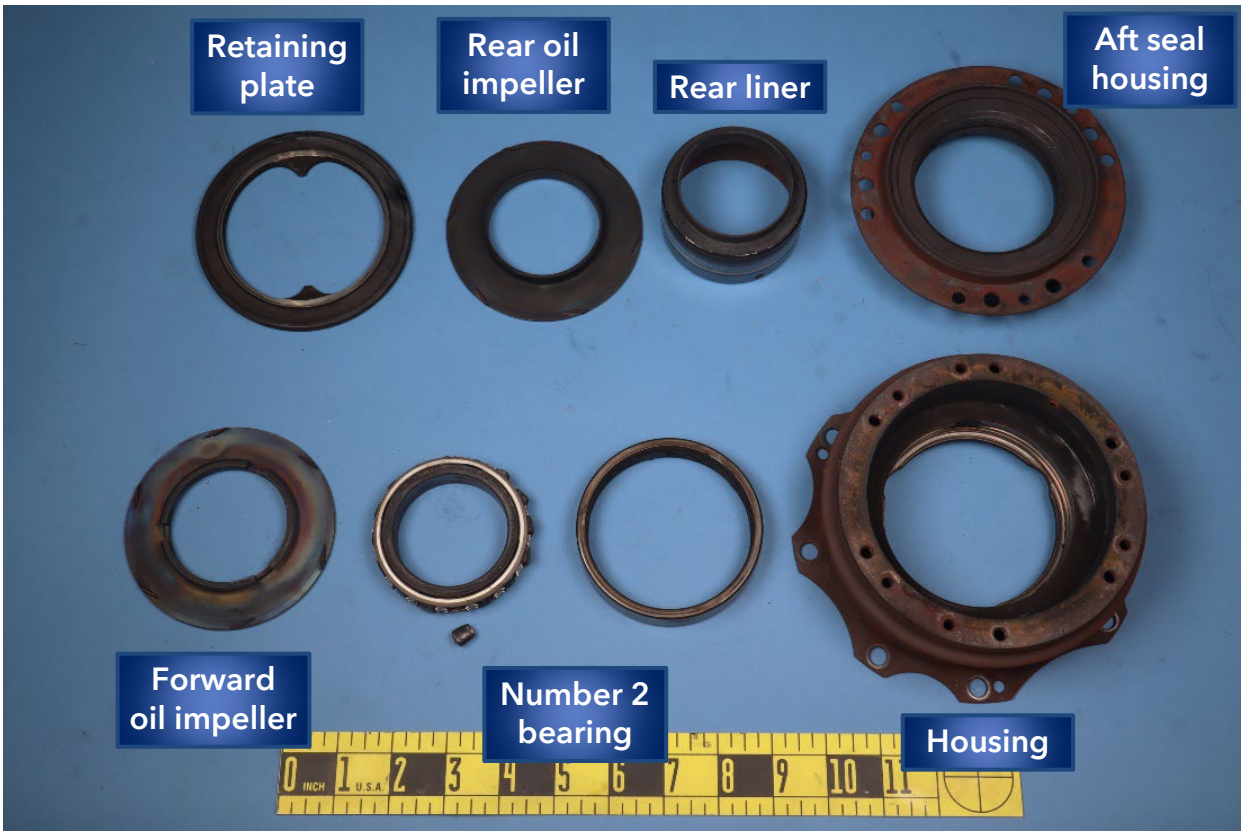

Figure 2. Number 2 bearing and associated components as received.

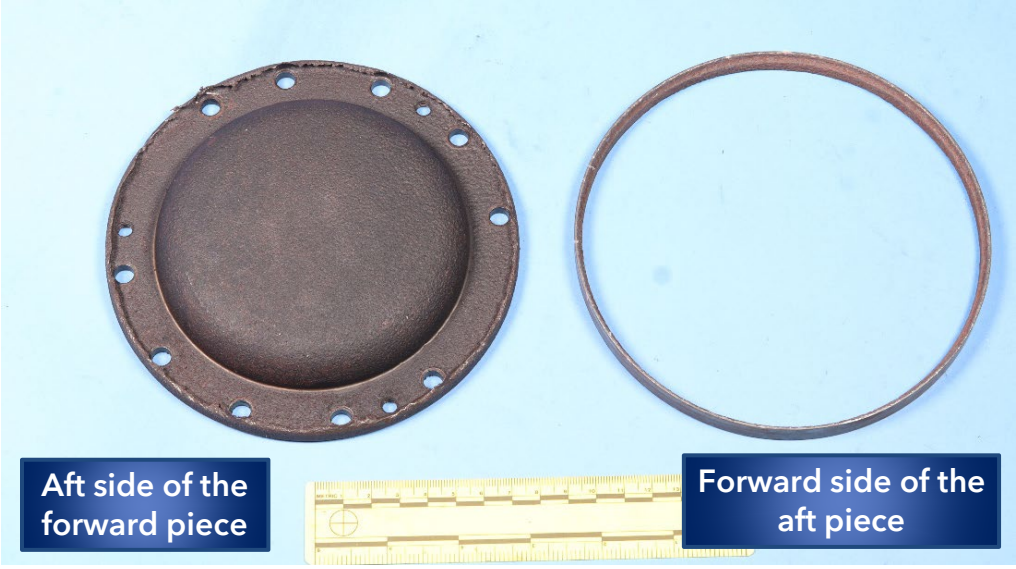

Figure 3. Rear bearing cover as received.

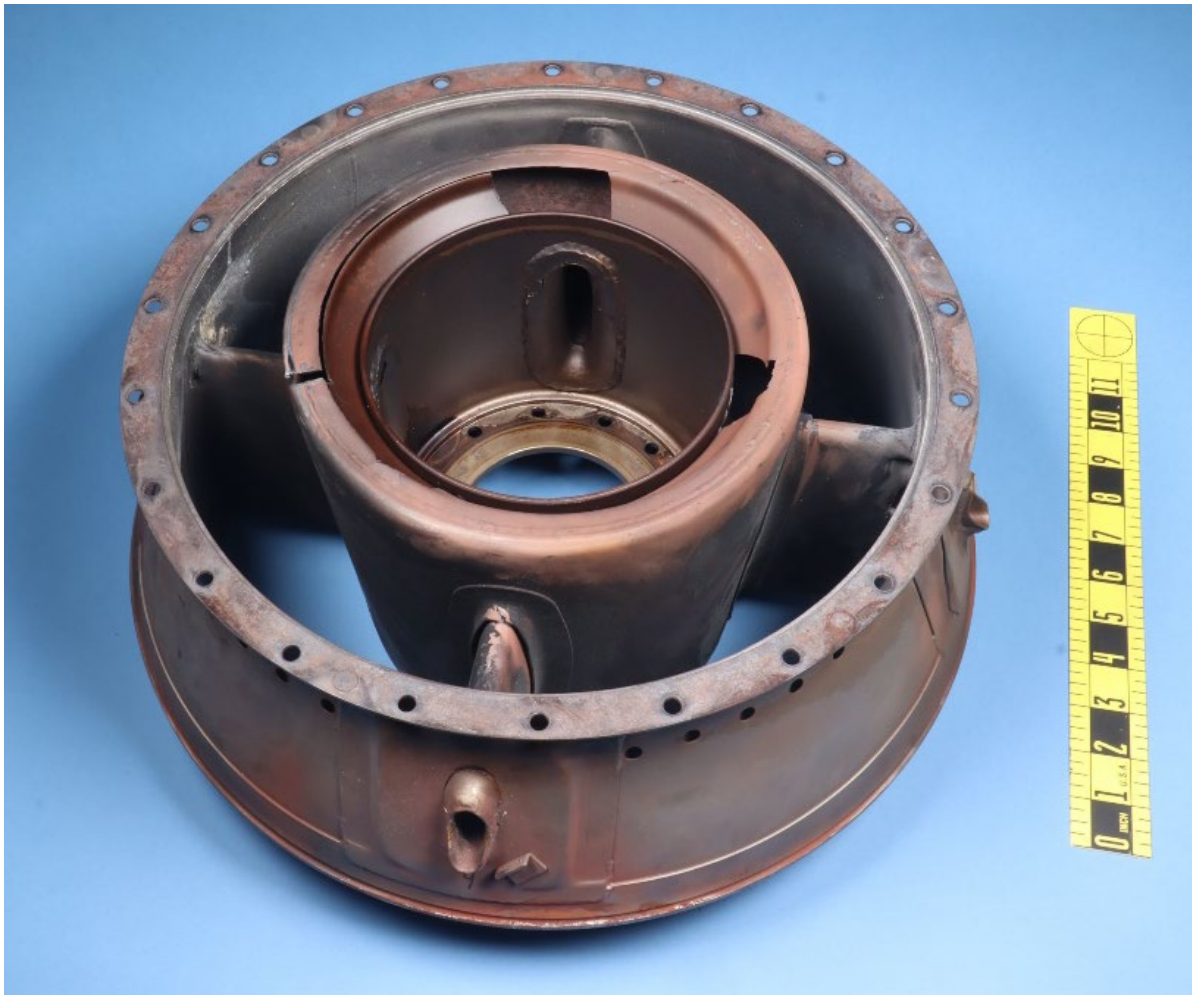

Figure 4. Exhaust diffuser as received.

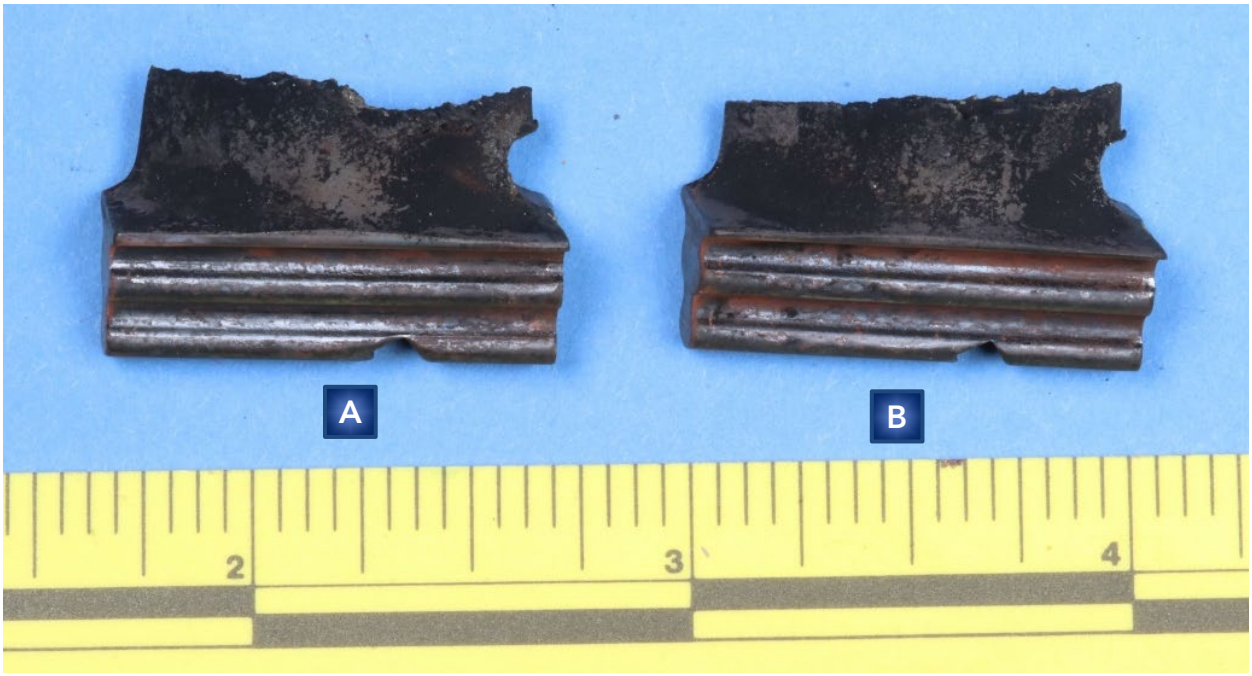

Figure 5. PT blade root fragments as received.

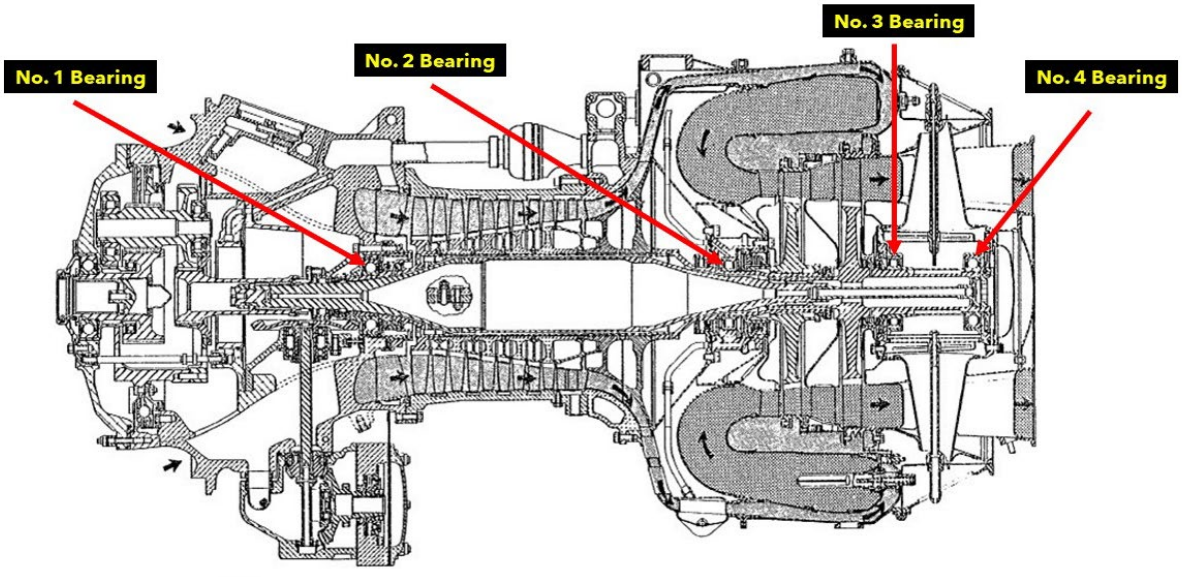

Figure 6. Diagram of a T53-L-11 engine sectioned longitudinally. Unlabeled black arrows indicate the direction of air flow through the engine.

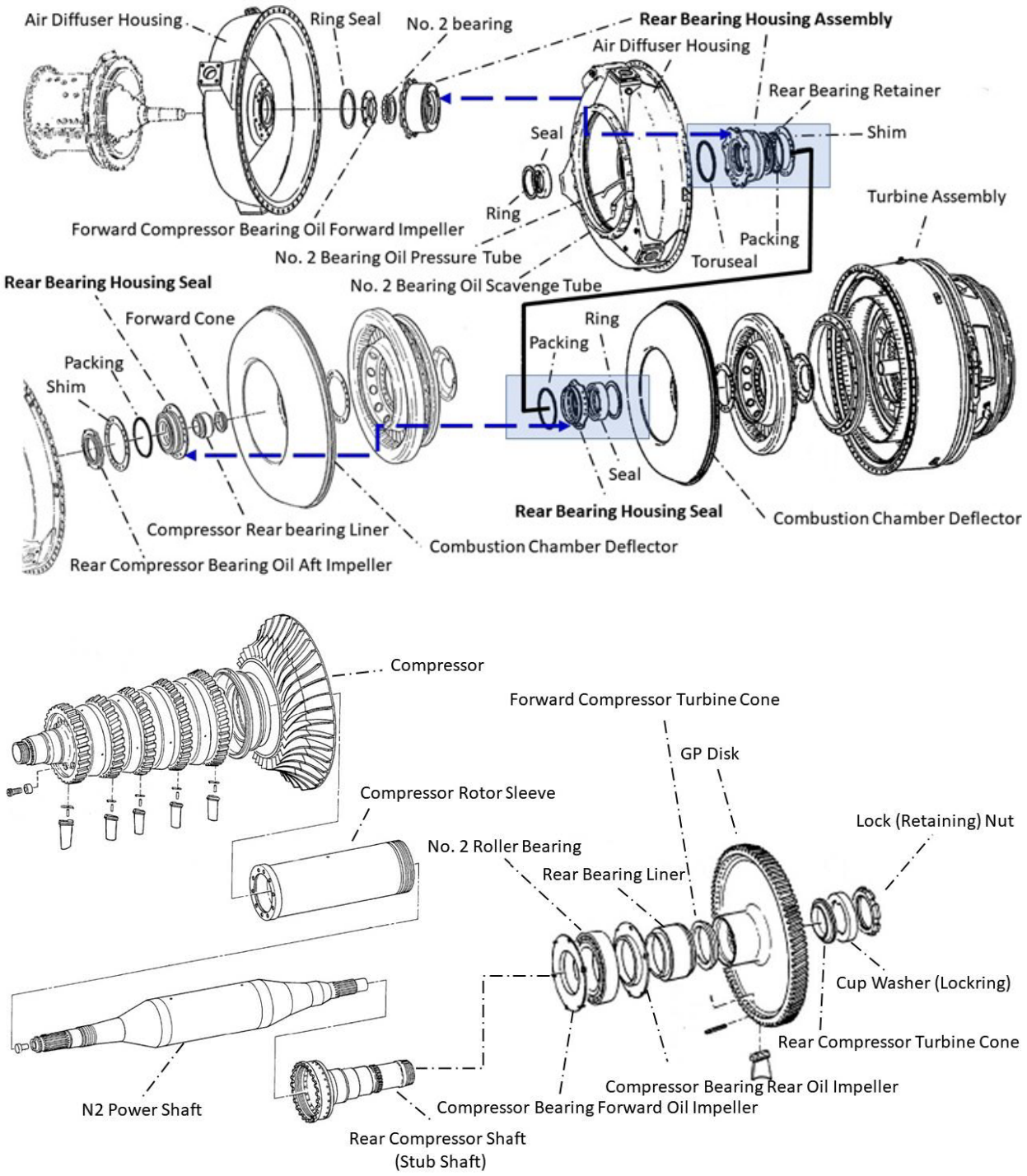

Figure 7. Assembly part diagrams of the number 2 bearing and associated non-rotating parts (above) and rotating parts (below). (Provided courtesy of Ozark Aeroworks and modified by NTSB.)

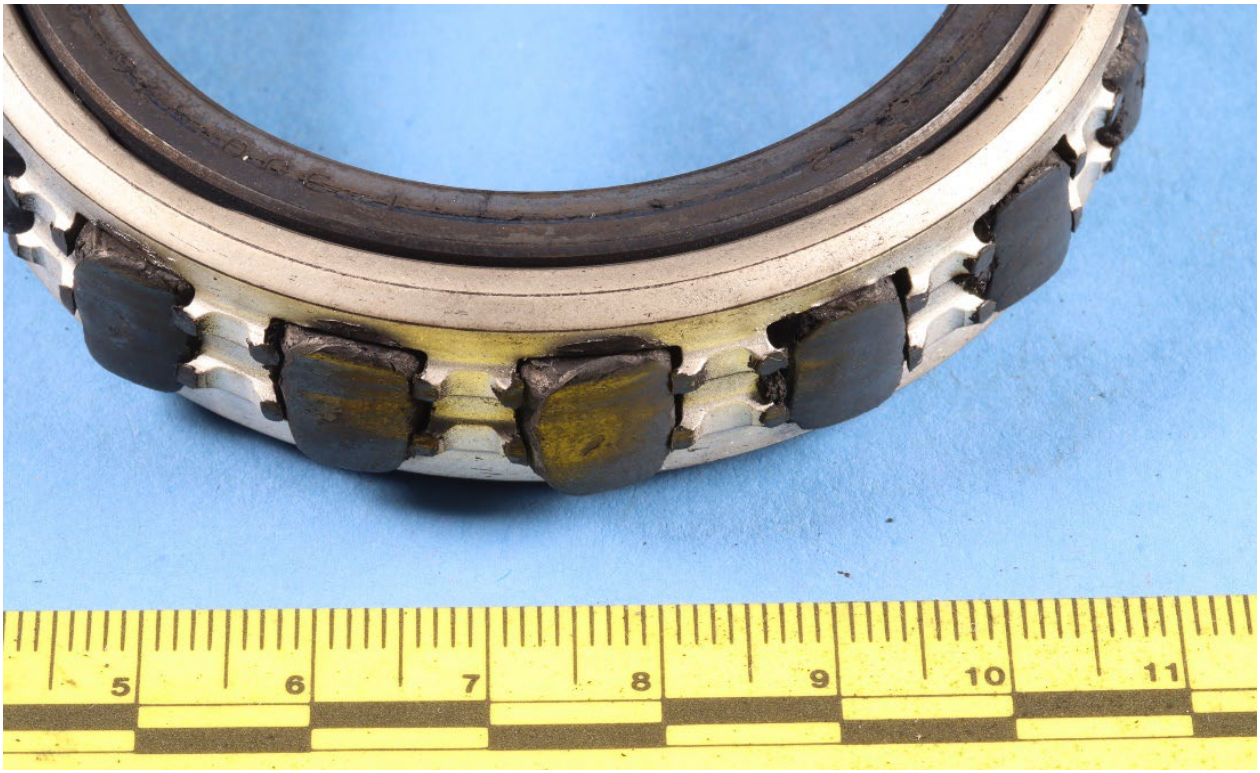

Figure 8. Number 2 bearing inner race, cage, and rolling elements (metric side of ruler shown).

Figure 9. Number 2 bearing outer race.

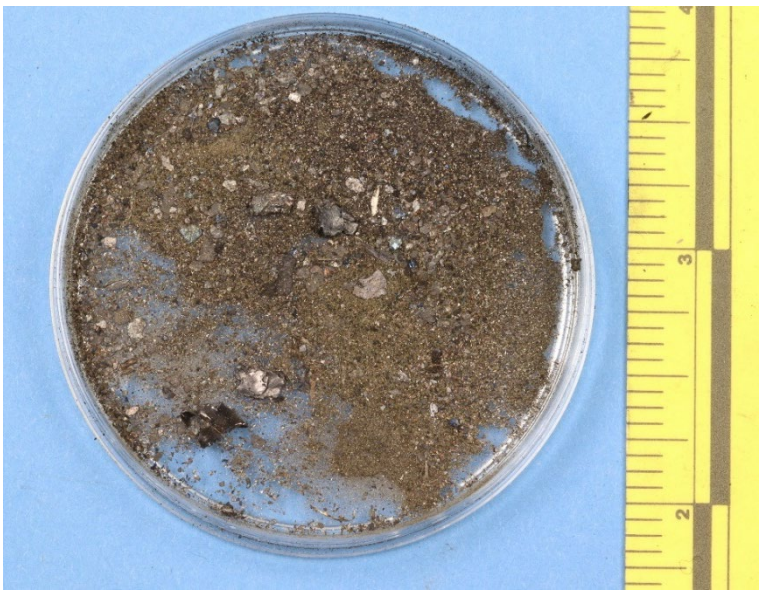

Figure 10. Debris removed from the air diffuser scavenge oil tube after cutting using an abrasive cutting tool.

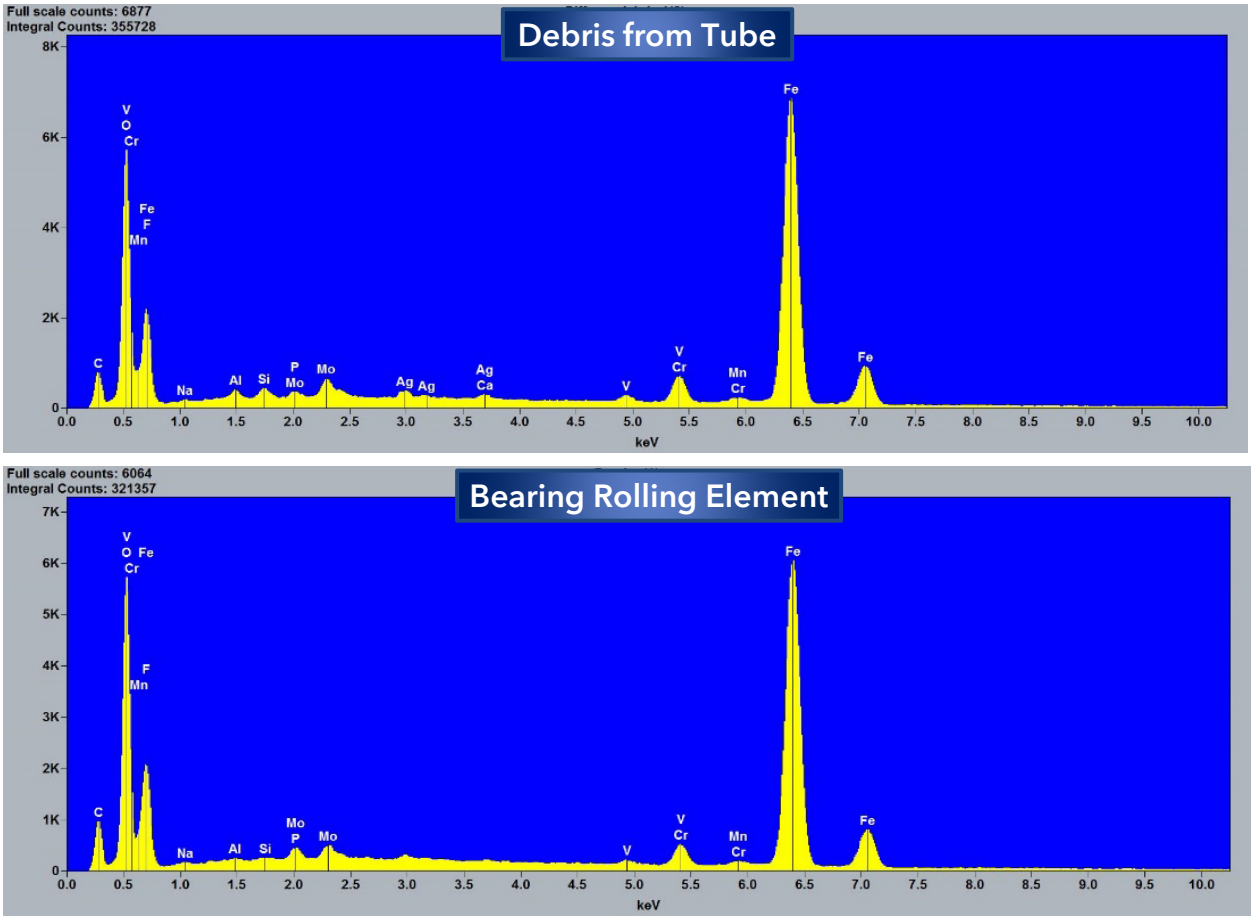

Figure 11. EDS spectrum of larger debris pieces from the oil scavenge tube (upper spectrum) and a rolling element from the number 2 bearing (lower spectrum).

Figure 12. Forward oil impeller (metric side of ruler shown).

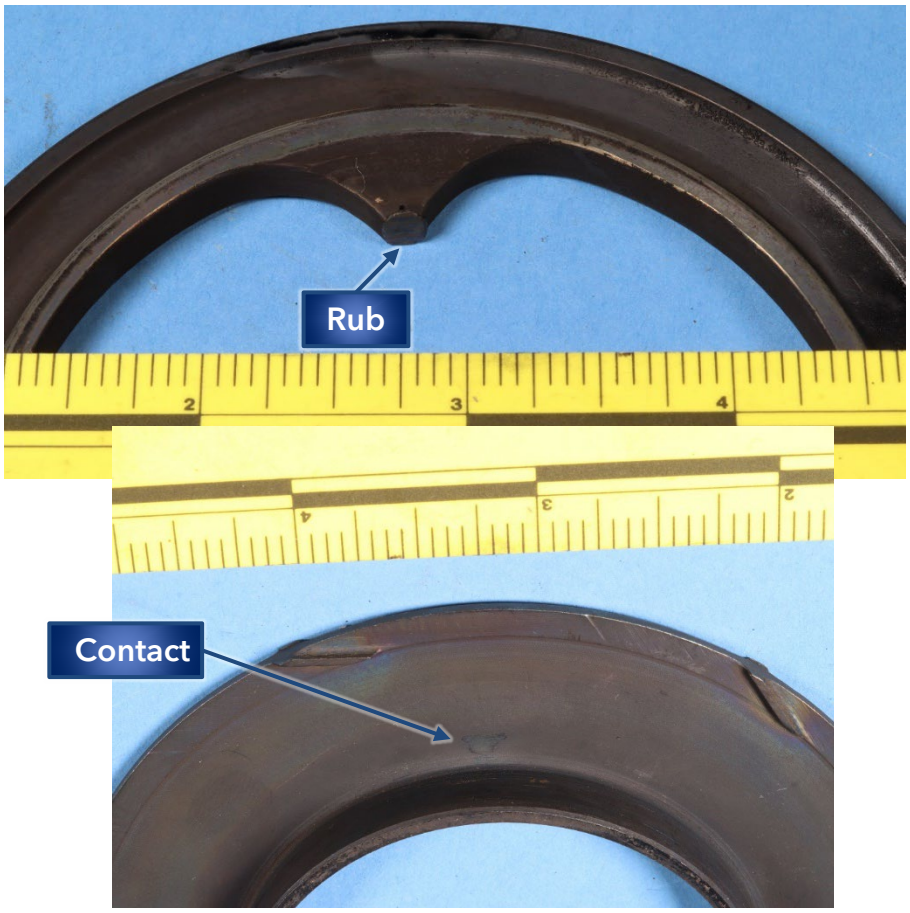

Figure 13. Retaining plate (above) and aft oil impeller (below).

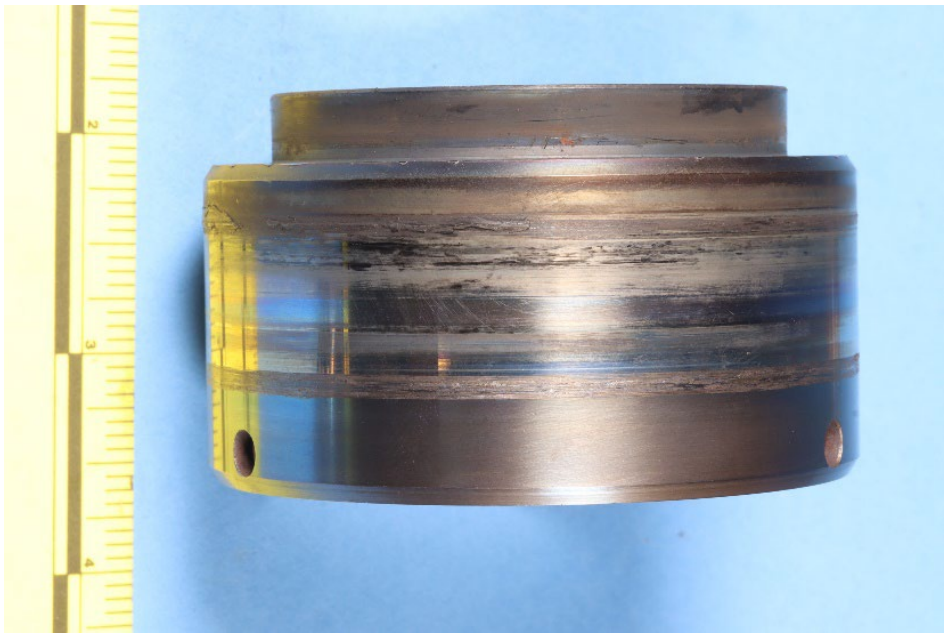

Figure 14. Rear liner.

Figure 15. Aft seal.

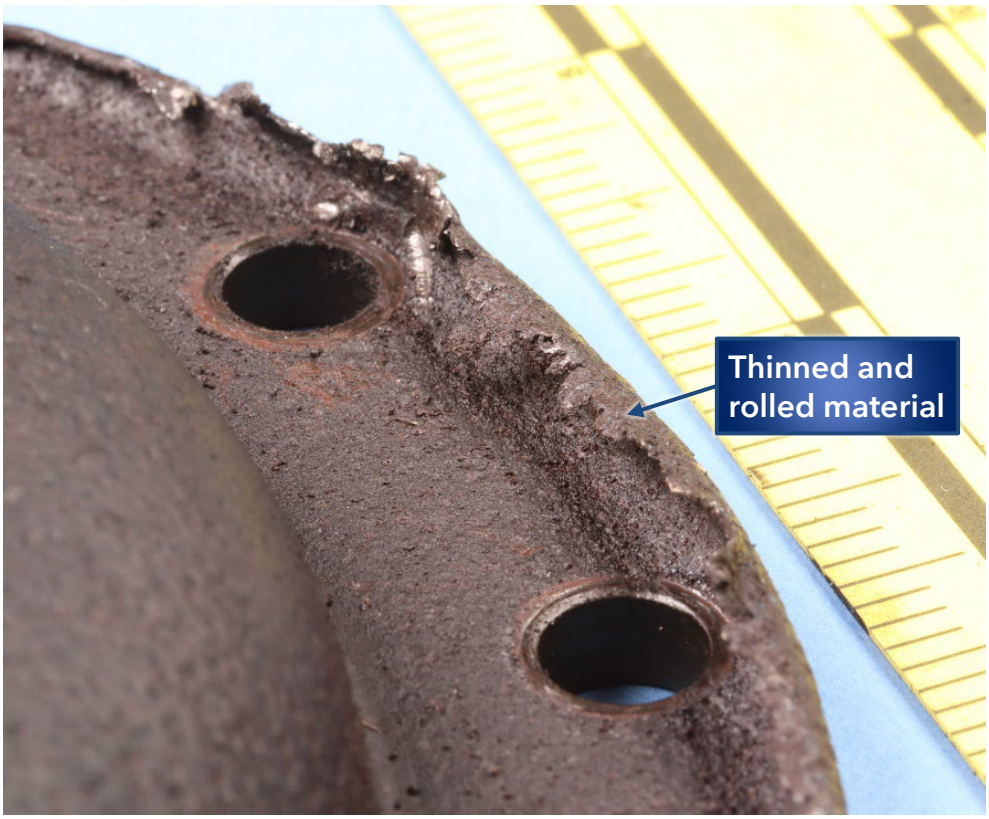

Figure 16. Aft side of the rear bearing cover showing thinned and rolled material at the flange separation around the outer diameter.

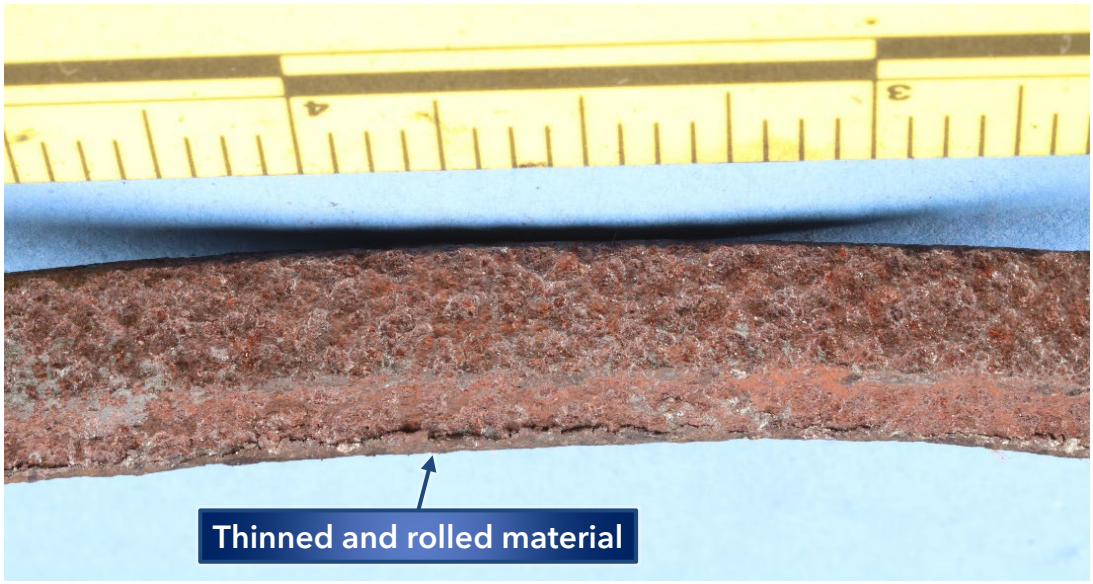

Figure 17. Rear bearing cover aft flange inner diameter face showing thinned and rolled material at the forward edge.

Figure 18. Piece of the rear bearing cover outer diameter flange cut from the forward piece showing the flange remnant surface on the inside of the curl.

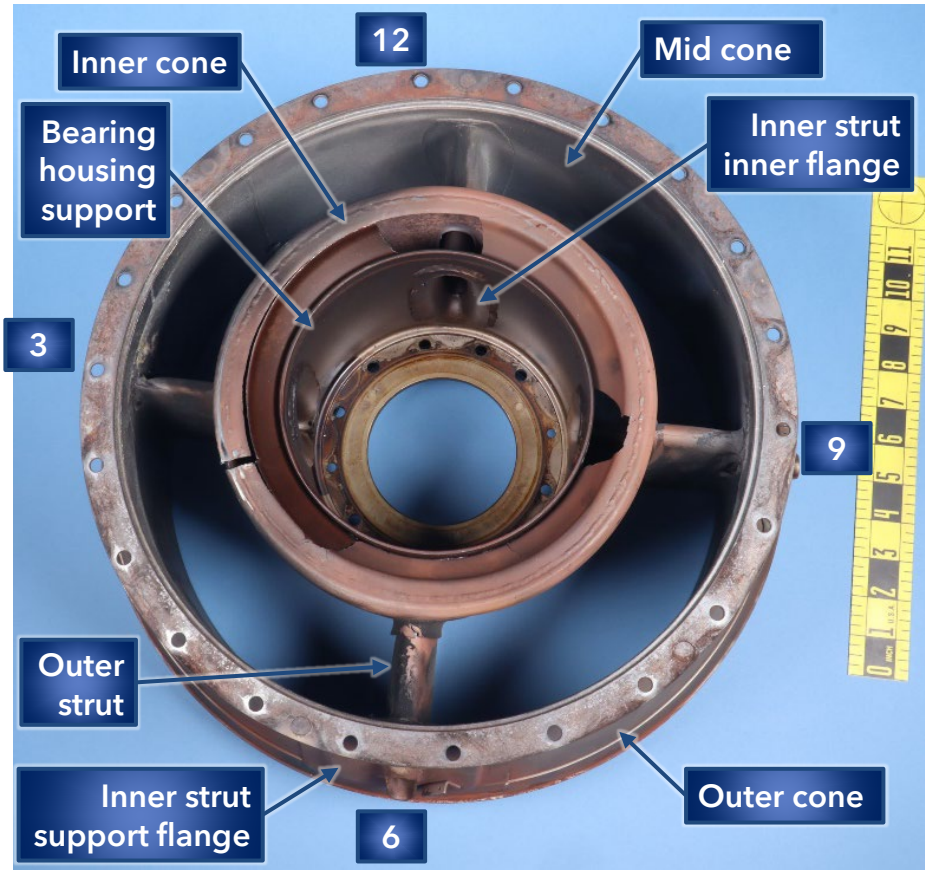

Figure 19. Forward side of the aft diffuser housing.

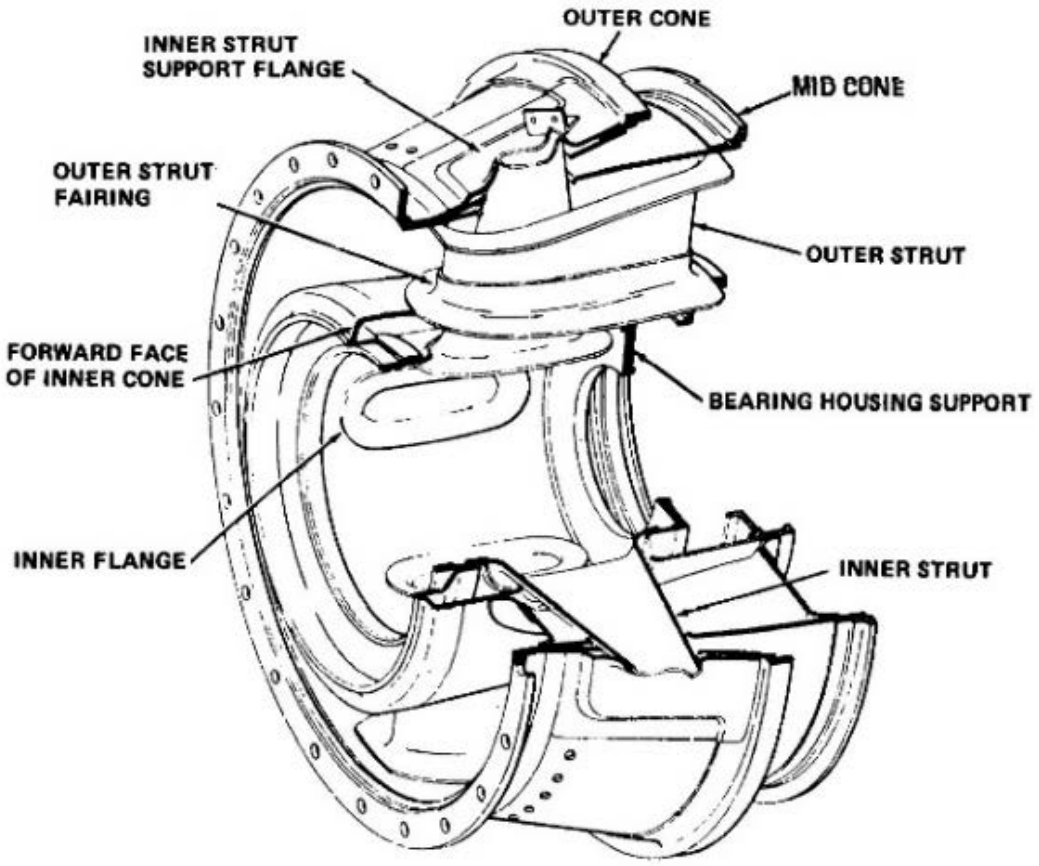

Figure 20. Exhaust diffuser cutaway diagram. (Provided courtesy of Ozark Aeroworks.)

Figure 21. Cracks at the leading edges of two outer struts where they attached to the mid cone at the 12 o'clock and 3 o'clock positions.

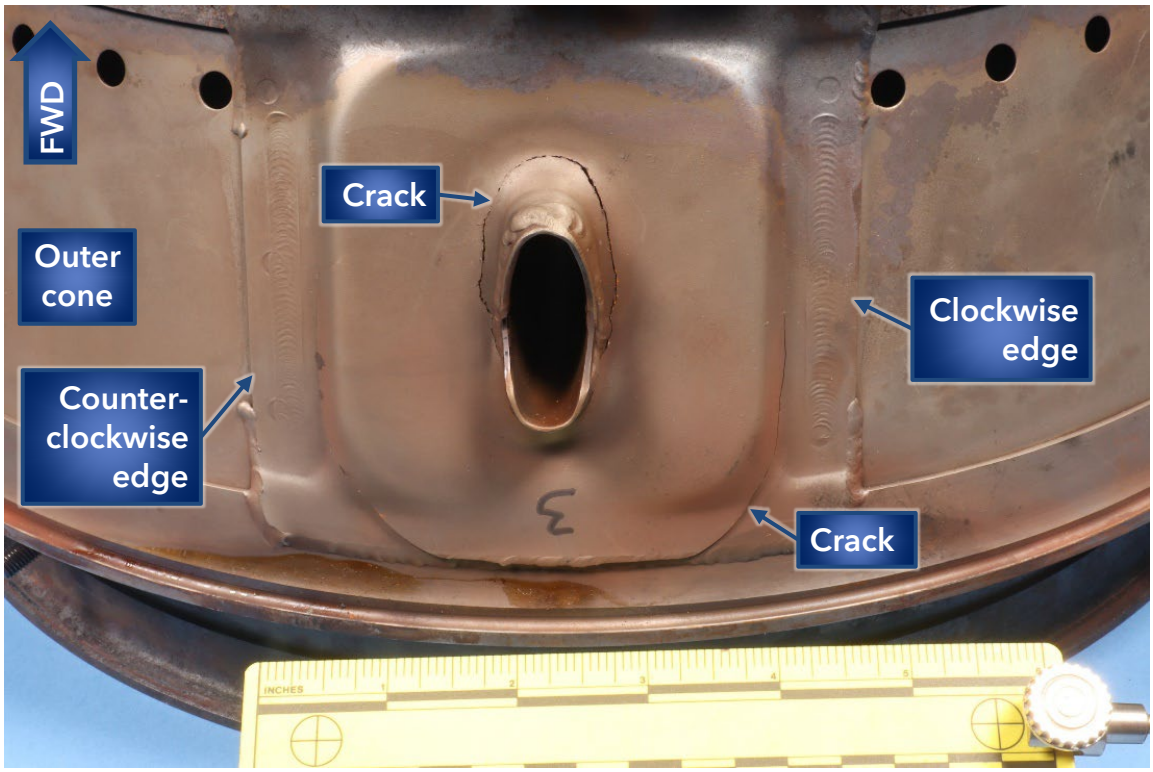

Figure 22. Number 3 inner strut support flange on the outer cone showing cracks around the strut attachment and at the aft edge of the flange.

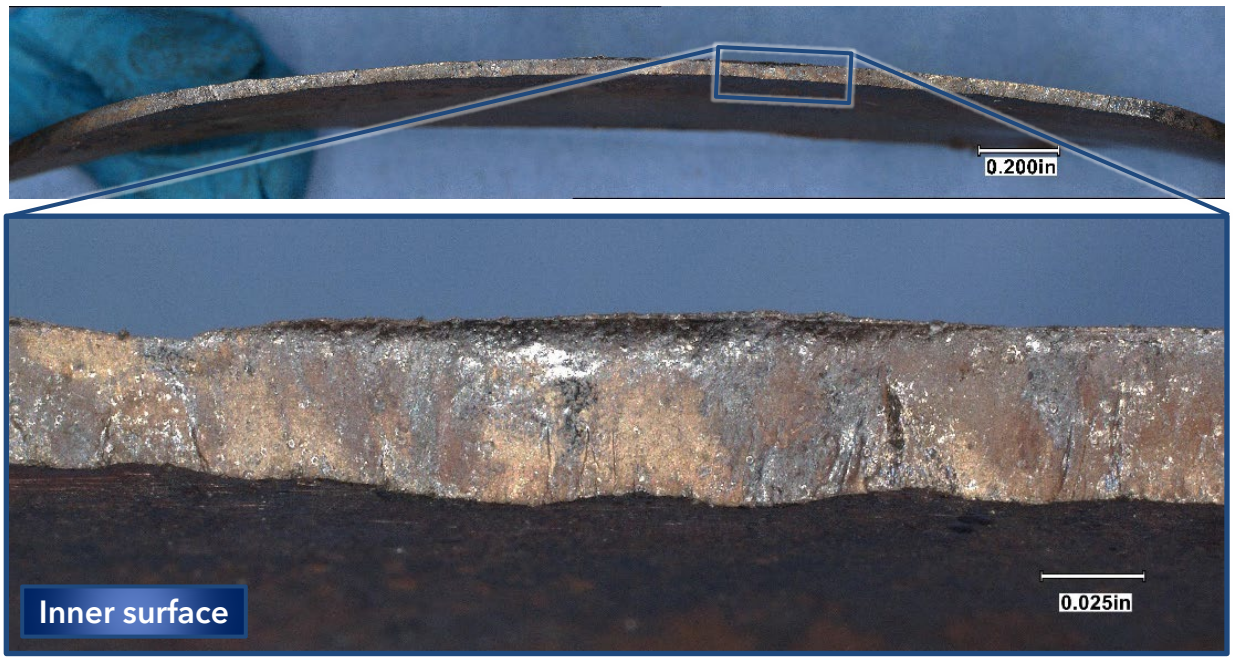

Figure 23. Fracture surface for the number 12 inner strut support flange crack at the aft edge of the flange.

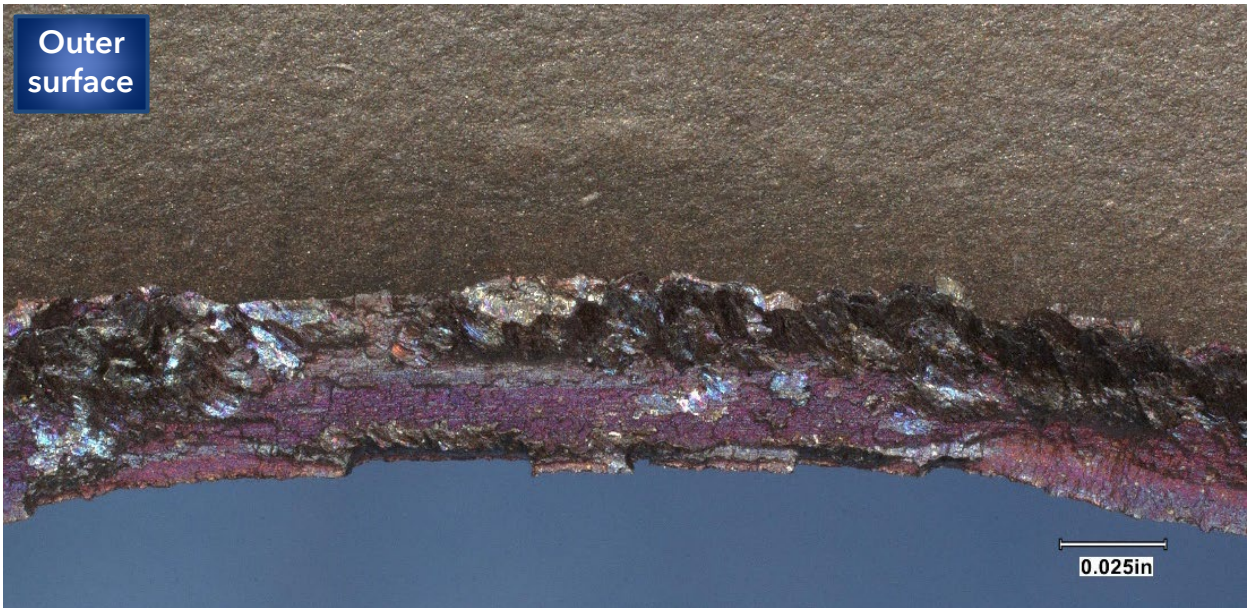

Figure 24. Fracture surface for the inner strut support flange crack at the inner strut attachment location (9 o'clock position).

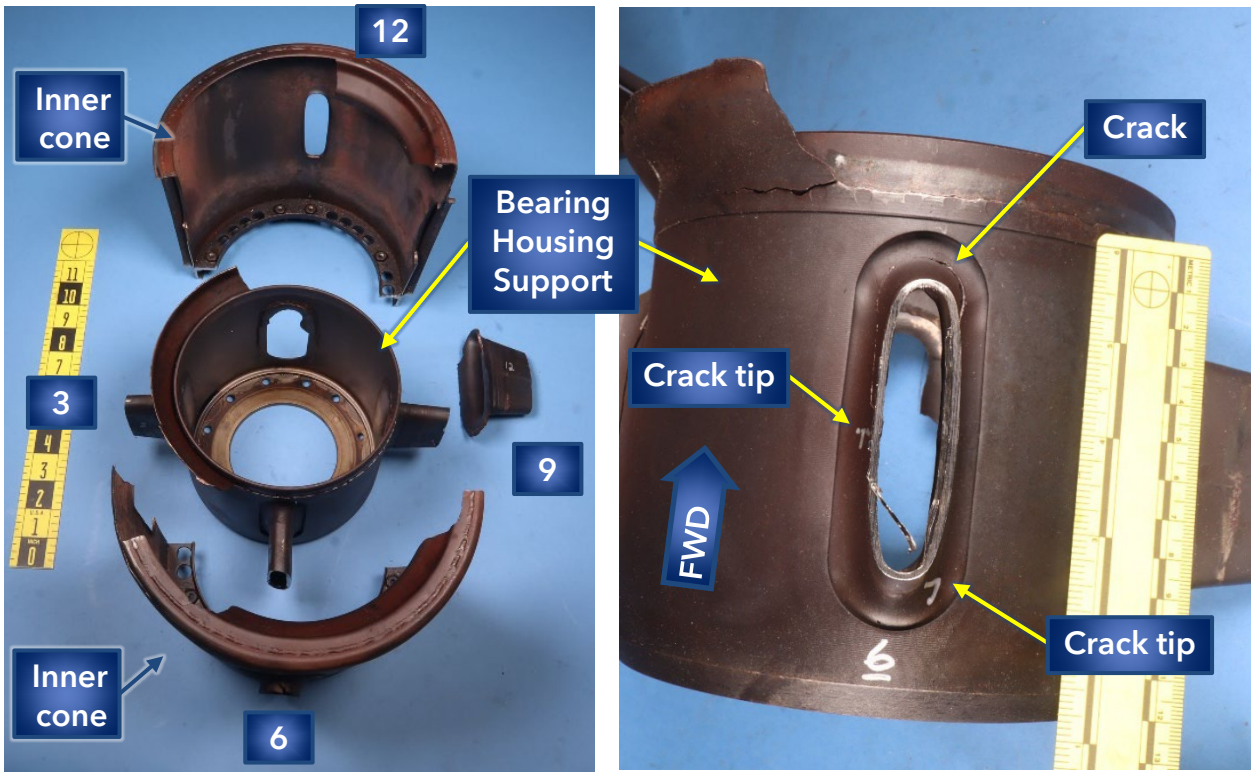

Figure 25. Views of the bearing housing support and inner struts after separating the inner cone from the support.

Figure 26. Inner ends of the inner struts after cutting from the bearing housing support (upper left). Closer views of fractures through the inner strut inner flanges at the 12 o'clock (upper right) and 6 o'clock (lower right and lower center) positions.

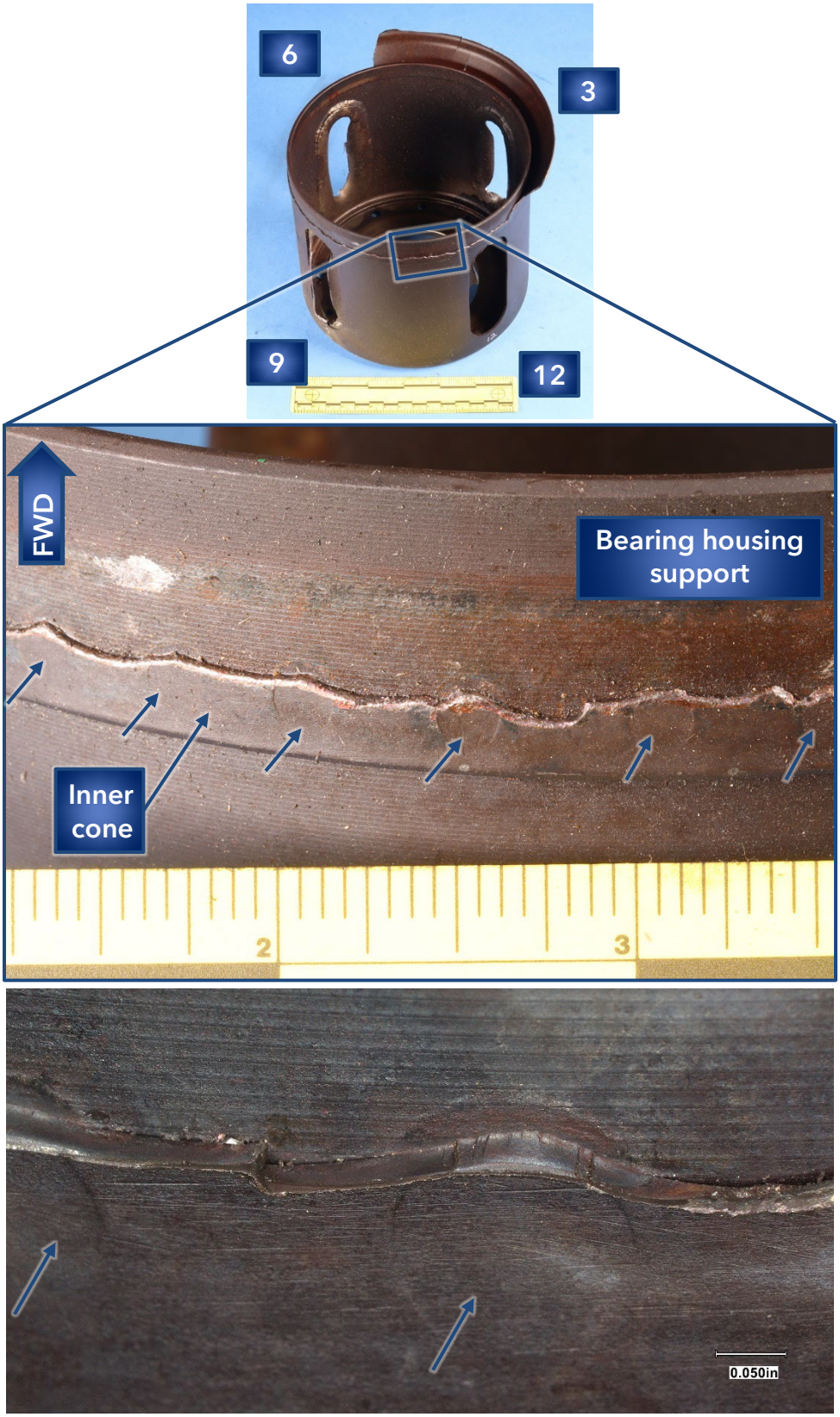

Figure 27. Bearing housing support with attached inner cone piece. Arrows indicate spot welds attaching the inner cone to the outer surface of the support.

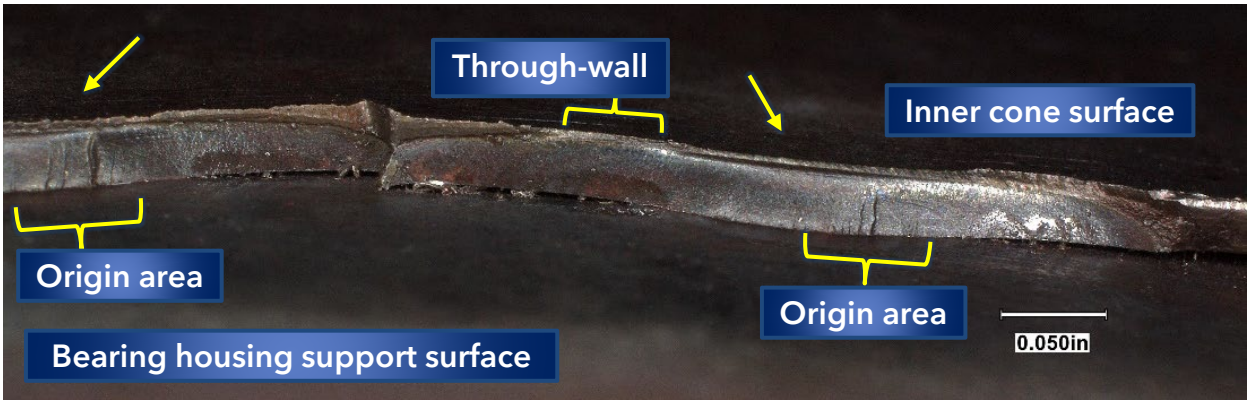

Figure 28. Portion of the fracture surface through the inner cone at the spot welds to the bearing housing support (viewed looking aft). Unlabeled arrows point to locations of spot welds on the shadowed inner cone surface.

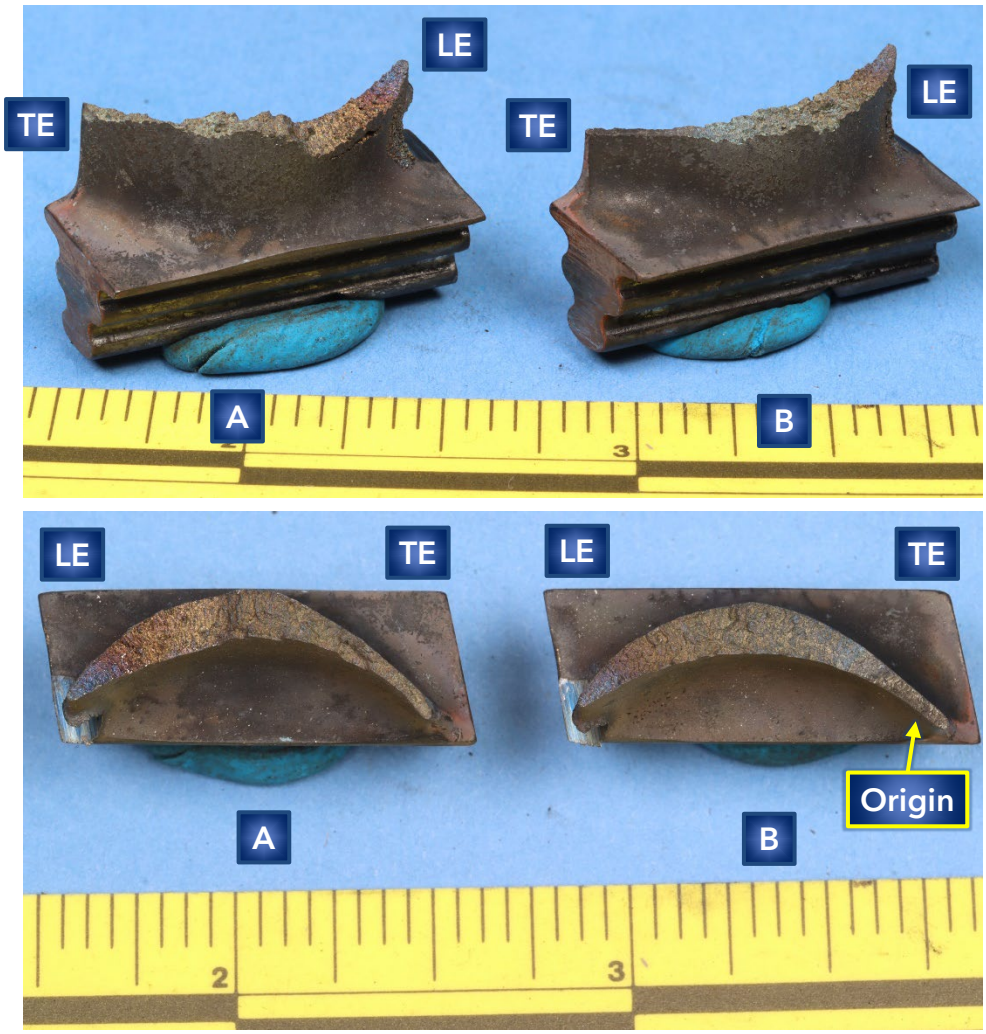

Figure 29. PT blades A and B after cleaning in a solution of Alconox and water using an ultrasonic cleaner.

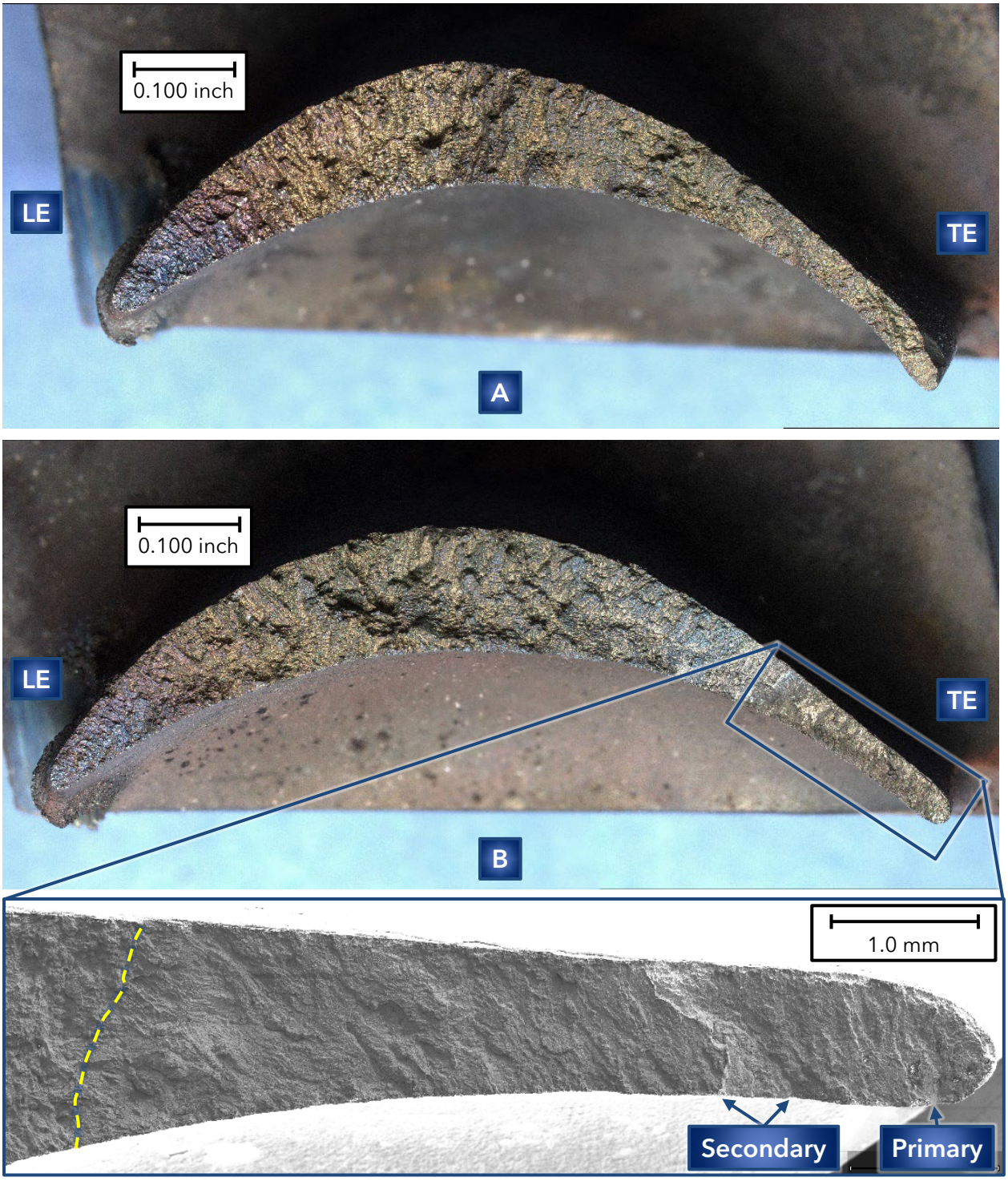

Figure 30. Optical images of PT blades A and B fracture surfaces (upper images) and a stitched montage SEM image of the blade B trailing edge showing primary and secondary fatigue origin areas (lower image). A dashed line in the SEM image indicates the fatigue boundary.

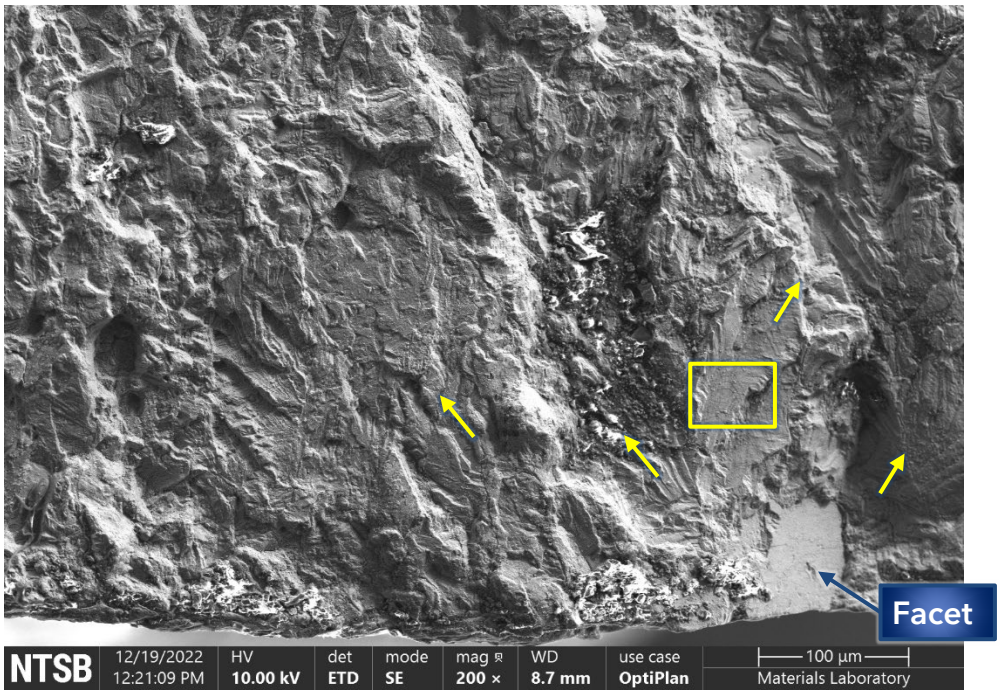

Figure 31. SEM image of fatigue features at the primary origin area on the PT blade B fracture surface. Arrows indicate fracture propagation directions emanating from smooth facet at the primary origin.

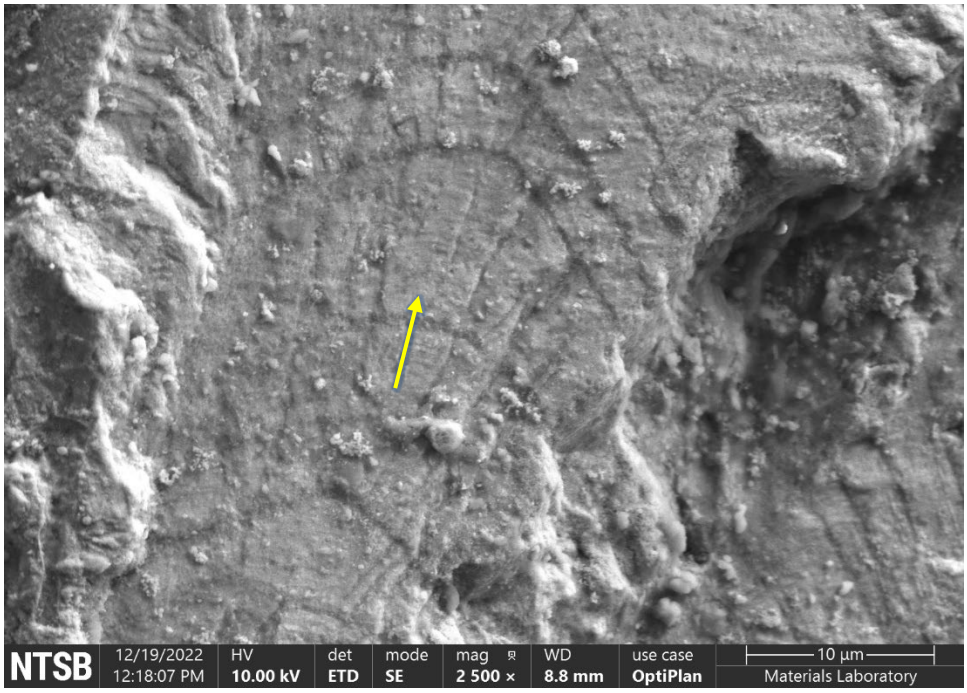

Figure 32. Fatigue features within the rectangular region shown in the previous figure. An unlabeled arrow indicates the local propagation direction.

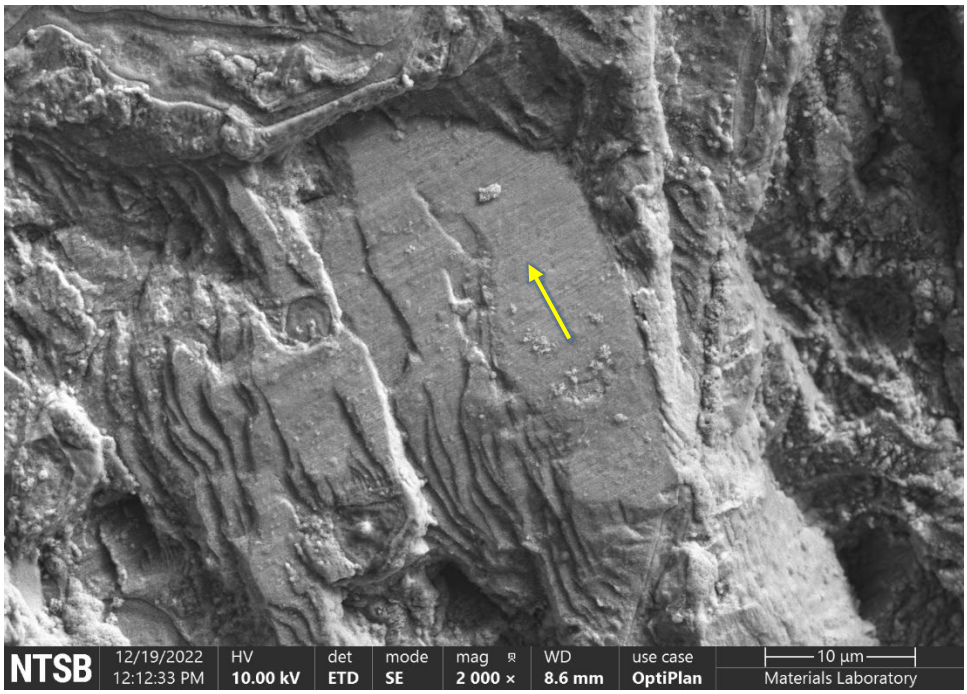

Figure 33. SEM image of fatigue features observed on the PT blade B fracture surface approximately 1.25 millimeters from the primary origin. An unlabeled arrow indicates the local propagation direction.

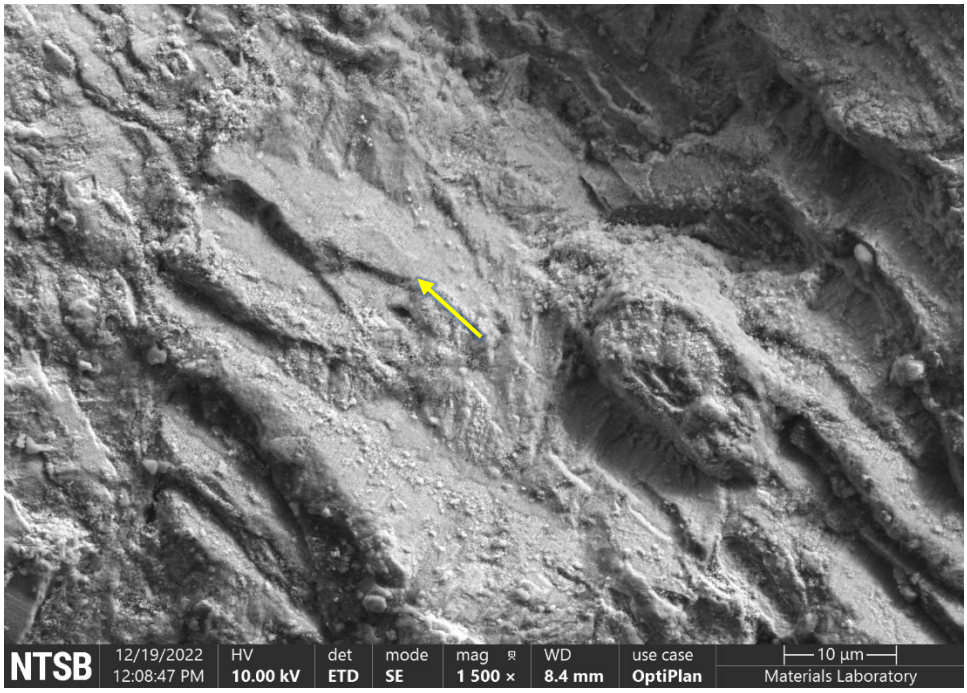

Figure 34. SEM image of fatigue features observed on the PT blade B fracture surface approximately 1.54 millimeters from the primary origin. An unlabeled arrow indicates the local propagation direction.

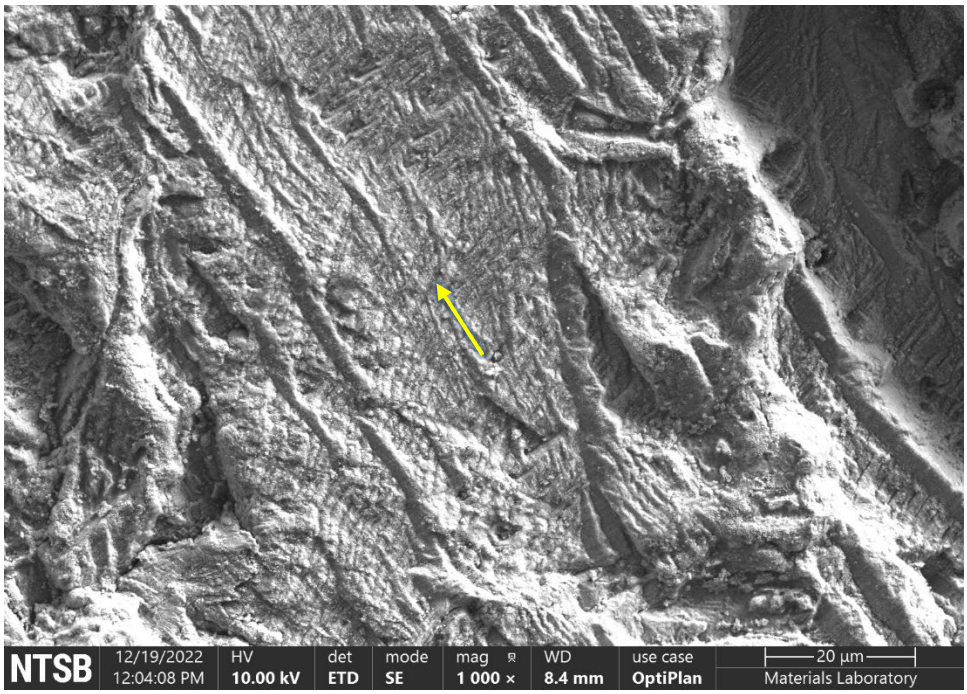

Figure 35. SEM image of fatigue features observed on the PT blade B fracture surface approximately 2.31 millimeters from the primary origin. An unlabeled arrow indicates the local propagation direction.

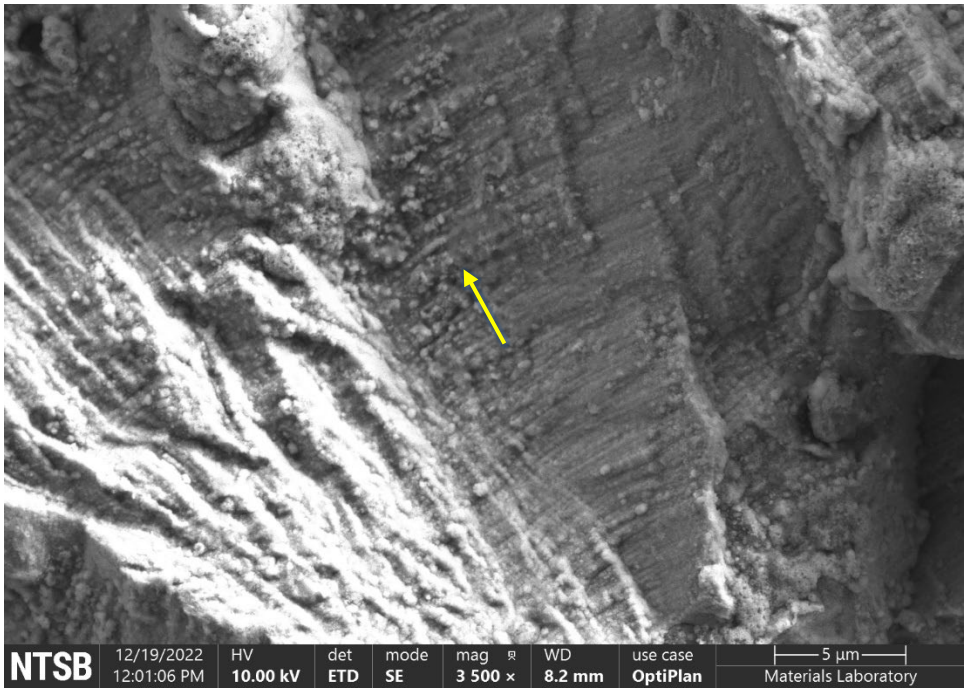

Figure 36. SEM image of fatigue features observed on the PT blade B fracture surface approximately 3.23 millimeters from the primary origin. An unlabeled arrow indicates the local propagation direction.

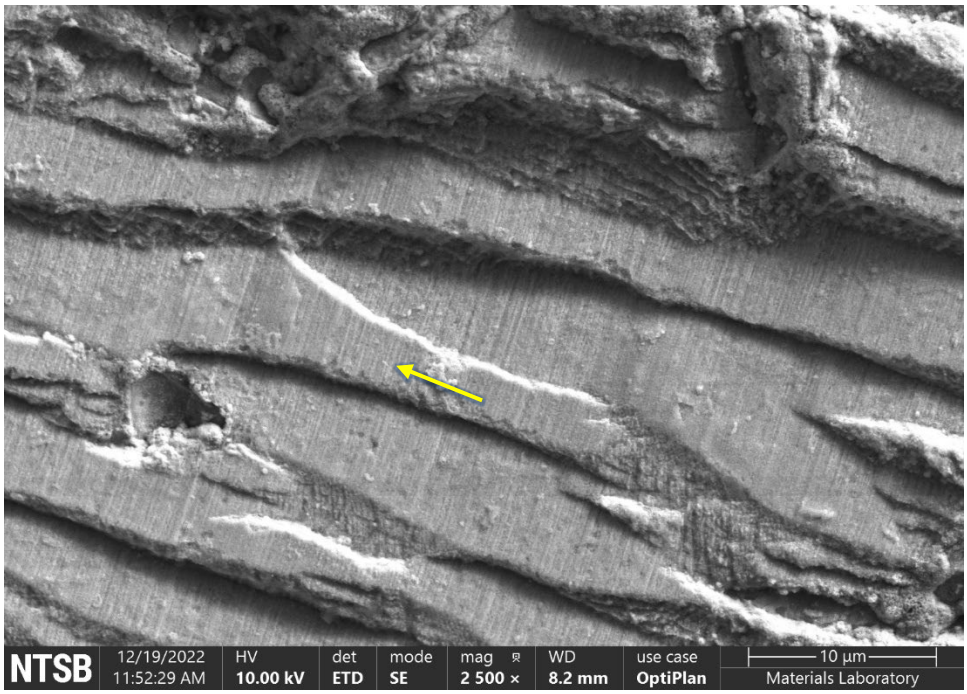

Figure 37. SEM image of fatigue features observed on the PT blade B fracture surface approximately 4.36 millimeters from the primary origin. An unlabeled arrow indicates the local propagation direction.

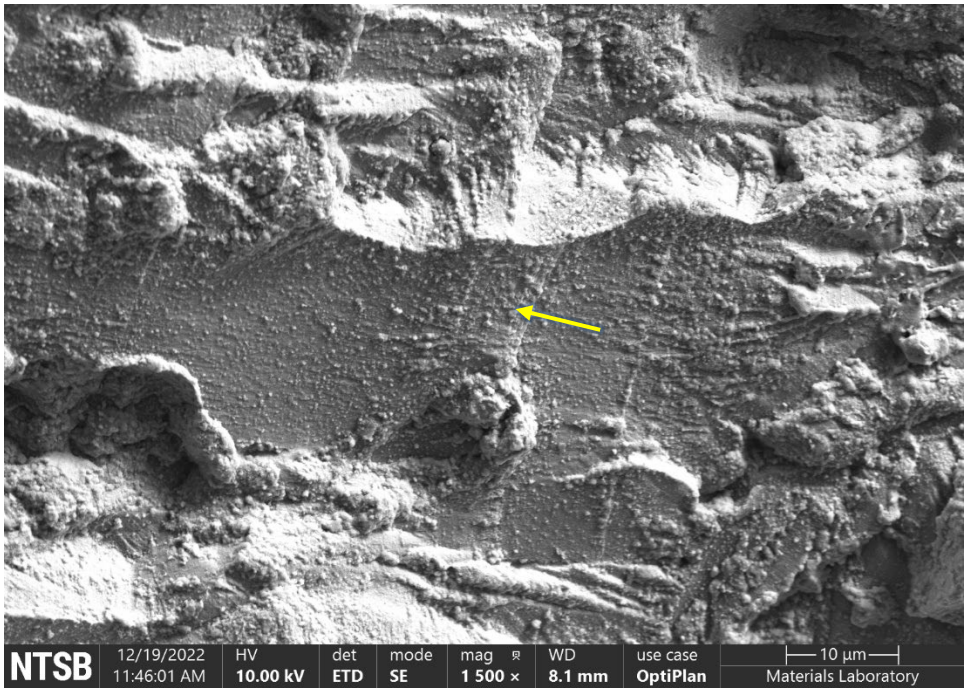

Figure 38. SEM image of fatigue features observed on the PT blade B fracture surface approximately 4.94 millimeters from the primary origin. An unlabeled arrow indicates the local propagation direction.

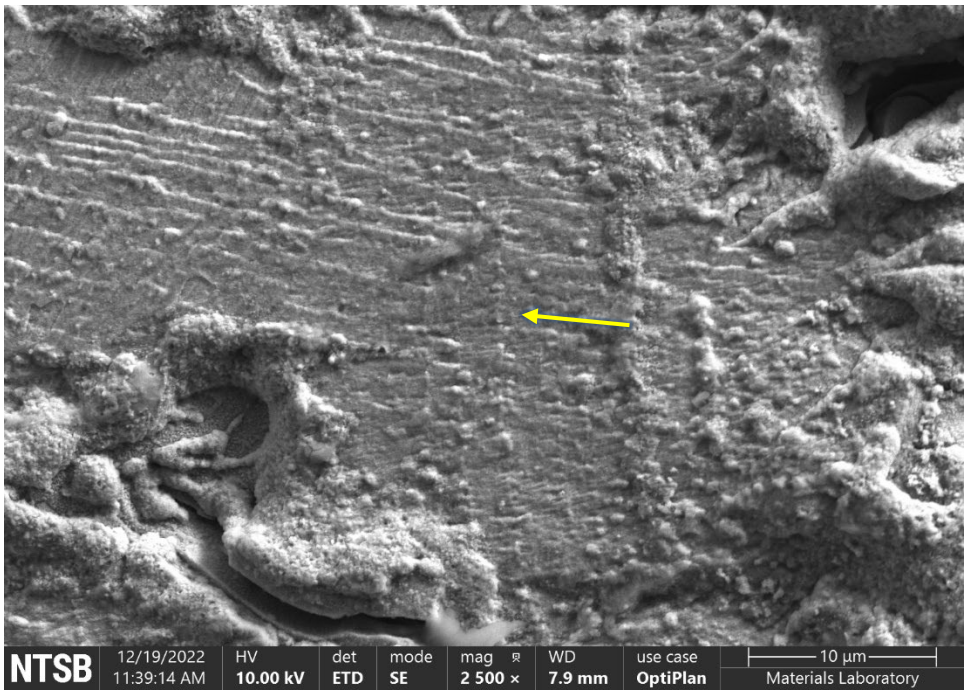

Figure 39. SEM image of fatigue features observed on the PT blade B fracture surface approximately 5.45 millimeters from the primary origin. An unlabeled arrow indicates the local propagation direction.

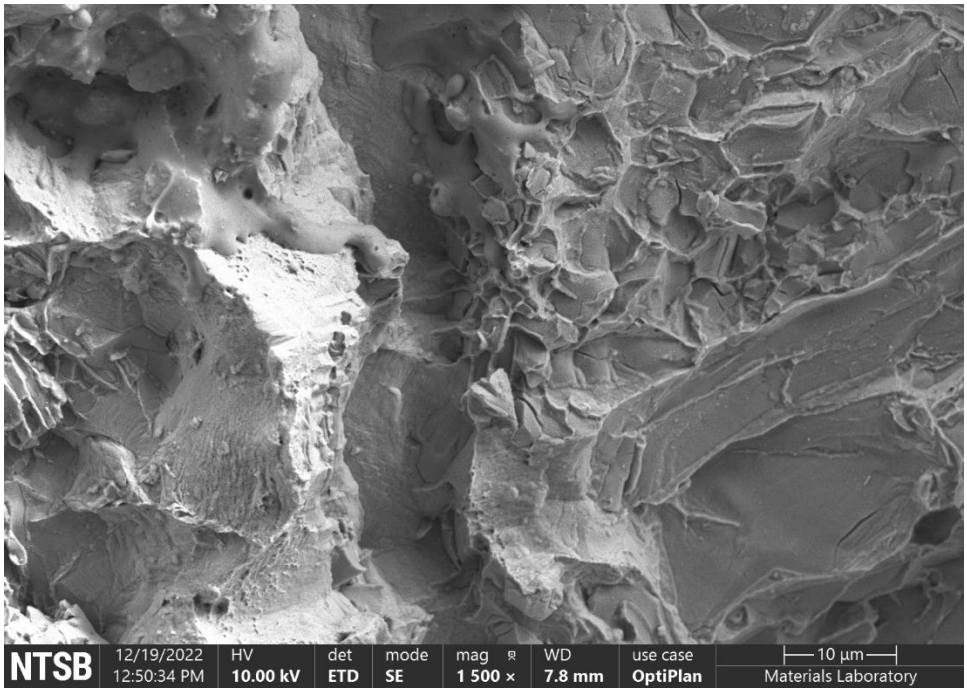

Figure 40. SEM image of typical overstress features on the PT blade B fracture surface.